

# Shape-Based Algorithm for Automated Design of Low-Thrust, Gravity-Assist Trajectories

Anastassios E. Petropoulos\* and James M. Longuski†  
*Purdue University, West Lafayette, Indiana 47907-1282*

Given the benefits of coupling low-thrust propulsion with gravity assists, techniques for easily identifying candidate trajectories would be extremely useful to mission designers. The computational implementation of an analytic, shape-based method for the design of low-thrust, gravity-assist trajectories is described. Two-body motion (central body and spacecraft) is assumed between the flybys, and the gravity-assists are modeled as discontinuities in velocity arising from an instantaneous turning of the spacecraft's hyperbolic excess velocity vector with respect to the flyby body. The method is augmented by allowing coast arcs to be patched with thrust arcs on the transfers between bodies. The shape-based approach permits not only rapid, broad searches over the design space, but also provides initial estimates for use in trajectory optimization. Numerical examples computed with the shape-based method, using an exponential sinusoid shape, are presented for an Earth–Mars–Ceres rendezvous trajectory and an Earth–Venus–Earth–Mars–Jupiter flyby trajectory. Selected trajectories from the shape-based method are successfully used as initial estimates in an optimization program employing direct methods.

## Nomenclature

$a$	= thrust acceleration normalized by local gravitational acceleration
$a_{0P}$	= zeroth-order constant coefficient for out-of-plane $a$
$b_0$	= first-order constant coefficient for out-of-plane $a$
$d_i$	= difference in inverse radii, $m^{-1}$
$F$	= thrust acceleration, $ms^{-2}$
$f_h$	= thrust acceleration along spacecraft's orbital angular momentum, $ms^{-2}$
$h_x$	= spacecraft specific orbital angular momentum, $x$ component, $m^2s^{-2}$
$h_y$	= spacecraft specific orbital angular momentum, $y$ component, $m^2s^{-2}$
$I_{sp}$	= specific impulse, s
$i$	= inclination, rad
$k_0$	= scale parameter for the exponential sinusoid, m
$k_1$	= dynamic range parameter for the exponential sinusoid
$k_2$	= winding parameter for the exponential sinusoid
$k_{12s}$	= $k_1 k_2^2 s$
$\dot{m}$	= propellant mass flow rate, $mg/s$
$n$	= integer
$P$	= power, kW
$p$	= semilatus rectum, m
$r$	= radial distance from the central body, m
$r_B$	= radial distance of flyby body (or switch point) from central body at time of flyby (or thrust switch on/off), m
$s$	= $\sin(k_2\theta + \phi)$

Presented as Paper 2001-467 at the AAS/AIAA Astrodynamics Specialists Conference, Québec City, QC, Canada, 30 July–2 August 2001; received 5 June 2002; revision received 28 July 2003; accepted for publication 1 August 2003. Copyright © 2003 by Anastassios E. Petropoulos and James M. Longuski. Published by the American Institute of Aeronautics and Astronautics, Inc., with permission. Copies of this paper may be made for personal or internal use, on condition that the copier pay the \$10.00 per-copy fee to the Copyright Clearance Center, Inc., 222 Rosewood Drive, Danvers, MA 01923; include the code 0022-4650/04 \$10.00 in correspondence with the CCC.

\*Ph.D. Candidate, School of Aeronautics and Astronautics; currently Senior Member of the Engineering Staff, Navigation and Mission Design Section, Jet Propulsion Laboratory, California Institute of Technology, Mail Stop 301-140L, 4800 Oak Grove Drive, Pasadena, CA 91109-8099. Member AIAA.

†Professor, School of Aeronautics and Astronautics. Associate Fellow AIAA.

$T$	= thrust, mN
$v_z$	= out-of-plane velocity, m/s
$v_\infty$	= hyperbolic excess velocity, m/s
$\alpha$	= thrust angle, rad
$\gamma$	= flight-path angle, rad
$\Delta V$	= velocity change, m/s
$\theta$	= polar angle, rad
$\mu$	= gravitational parameter of central body, $m^3s^{-2}$
$\rho$	= projected radius on the low-thrust reference plane, m
$\rho_n$	= lower bound for $\rho$ , m
$\rho_x$	= upper bound for $\rho$ , m
$\phi$	= phase angle for exponential sinusoid, rad; out-of-plane position angle, rad
$\omega$	= argument of periaxis, rad

## Subscripts

$A, B, \dots$	= value at points $A, B, \dots$
$\max$	= maximum value over the independent variable
$\min$	= minimum value over the independent variable

## Superscript

.	= derivative with respect to time
---	-----------------------------------

## Introduction

IT is well known that efficient, continuous-thrust propulsion and gravity assist each provide significant benefits in trajectory design. Furthermore, each has been demonstrated in practice: NASA's Deep Space 1 spacecraft<sup>1,2</sup> has recently provided the first validation of interplanetary use of solar electric propulsion, whereas gravity assists have been repeatedly used in the exploration of the solar system, perhaps most notably by Voyager II,<sup>3</sup> which was launched in 1977. The coupling of high-specific-impulse, low-thrust propulsion with gravity assists is a natural next step in the development of trajectory design techniques for deep space missions. In the literature, the design of such trajectories is typically treated as an optimization problem, which can be solved by a variety of techniques.<sup>4–14</sup> However, all of these techniques need some sort of initial guess for at least part of the solution, and even with such a guess, experience has shown that convergence to an optimal solution, particularly in the case of multiple gravity assists, is a formidable challenge. In this paper, rather than addressing the optimization of particular initial guesses, we present a shape-based method<sup>15,16</sup> for efficiently generating initial estimates for low-thrust, gravity-assist trajectories.

These initial estimates serve a twofold purpose: They provide mission designers with rapid, broad overviews of the trajectory design space<sup>16</sup> (hence the use of the word estimate rather than guess), and they provide a starting point for trajectory optimization.

In the shape-based approach, the powered spacecraft trajectory is assumed to be of a certain shape, with the requisite thrust profile determined therefrom. With the correct choice of shape, not only can we add to the small family of analytic solutions to the equations of motion (for example, Refs. 17–22), but we can also obtain trajectories with satisfactory performance and feasible, or near-feasible, thrust profiles. Here we consider cases where multibody effects are not significant, allowing the use of the simpler two-body equations of motion, with the gravity assists treated as discontinuities in velocity. In addition, we make the assumption that the spacecraft trajectory between gravity assists is roughly planar. Having studied a number of planar shapes,<sup>15,16,18,23</sup> we select the exponential sinusoid<sup>15,16,23</sup> as the most promising of these for representing the powered portion of flight between gravity-assist bodies. The out-of-plane motion required to encounter a gravity-assist or destination body is assumed to be small and is approximated through an analysis of the orbital angular momentum vector. We describe a computational method of solution of the resulting equations and the implementation of this method in a new software. Two examples of trajectory searches using the new software are presented for one-gravity-assist, Ceres rendezvous trajectories, and for three-gravity-assist, Jupiter-flyby trajectories, both over broad ranges in launch date and launch energy. The searches are automated in the sense that the software can find potentially thousands of trajectories over a large parameter space, based on a simple input file. In addition to the broad searches, we also present two sample trajectories computed with this method and use the two trajectories as initial estimates in a direct-optimization program, comparing one of them to an existing trajectory in the literature.

## Methodology

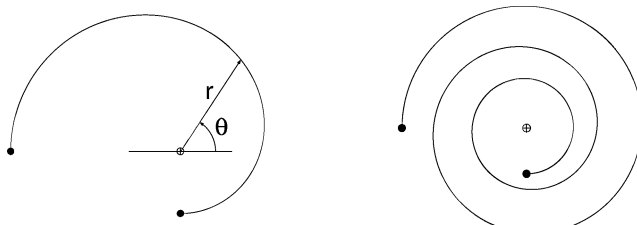
### Overview

In this section, we describe how exponential-sinusoid-based thrust arcs are incorporated into the Satellite Tour Design Program<sup>24–26</sup> (STOUR), to form a new program, STOUR-LTGA, which automatically searches for low-thrust, gravity-assist (LTGA) trajectories. As in STOUR, the user specifies a sequence of gravity-assist bodies, a range of launch dates, and a range of launch  $v_\infty$  for trajectories, subject to various constraints, such as time of flight (TOF) and propellant consumption constraints. In STOUR-LTGA, as in STOUR, the positions and velocities of the solar system bodies are modeled by polynomial representations, or, if the user so requests, by more accurate ephemeris data.

Previous papers<sup>15,16</sup> present an analysis of various thrust profiles that can be used to produce a trajectory of exponential sinusoid shape, given in polar coordinates ( $r, \theta$ ) by

$$r = k_0 \exp[k_1 \sin(k_2\theta + \phi)] \quad (1)$$

where  $k_0, k_1, k_2$ , and  $\phi$  are constants. Two examples of an exponential sinusoid, demonstrating the effect of the winding parameter  $k_2$ , are shown in Fig. 1. The dynamic range parameter  $k_1$  controls the ratio of the apoapsis distance to the periapsis distance. The parameter



a)  $k_2 = 2/3$

b)  $k_2 = 2/11$

Fig. 1 Sample exponential sinusoid shapes, shown from periapsis to apoapsis, for  $k_1 = 0.5$ .

$k_0$  is simply a scaling factor, and the phase angle  $\phi$  controls the orientation of the exponential sinusoid in the plane.

By thrust profile, we mean thrust direction and magnitude of the acceleration due to thrust as functions of position on the trajectory. Of the thrust profiles considered, we choose the tangential thrust case because this case 1) is the simplest analytic case, 2) is less prone to singularities, and 3) has tolerable thrust-acceleration levels and attractive velocity profiles for both flyby missions and rendezvous missions. By tangential thrust, we mean thrust along or against the velocity vector. Noteworthy is that the shape assumption with the tangential thrust assumption together dictate the magnitude of the thrust acceleration as a function of the shape parameters and the position on the shape. The familiar two-body equations of motion in polar coordinates are

$$\ddot{r} - r\dot{\theta}^2 + \frac{\mu}{r^2} = F \sin \alpha \quad (2)$$

$$\frac{1}{r} \frac{d}{dt}(r^2\dot{\theta}) = F \cos \alpha \quad (3)$$

where the overdot denotes differentiation with respect to time,  $\mu$  is the gravitational parameter of the central body–spacecraft system,  $F$  is the magnitude of the thrust acceleration, and  $\alpha$  is the thrust angle with respect to the local horizon. It is convenient to normalize  $F$  by the local gravitational acceleration:

$$a \equiv F/(\mu/r^2) \quad (4)$$

The normalized thrust acceleration  $a$  will thus be a small constant if  $F$  is small and drops off with  $1/r^2$ , as is roughly the case with power-limited solar electric propulsion.<sup>13</sup> The flight-path angle  $\gamma$ , namely the angle of the velocity vector with respect to the local horizon, given geometrically by  $\tan \gamma = (dr/d\theta)/r$ , is easily seen from the shape equation (1) to be

$$\tan \gamma = k_1 k_2 \cos(k_2\theta + \phi) \quad (5)$$

Then, the shape equation (1), the equations of motion (2) and (3) and the tangential thrust assumption yield the following analytic expressions for angular rate  $\dot{\theta}$  and normalized thrust acceleration:

$$\dot{\theta}^2 = \left( \frac{\mu}{r^3} \right) \frac{1}{\tan^2 \gamma + k_1 k_2^2 s + 1} \quad (6)$$

$$a = \frac{(-1)^n \tan \gamma}{2 \cos \gamma} \left[ \frac{1}{\tan^2 \gamma + k_1 k_2^2 s + 1} - \frac{k_2^2 (1 - 2k_1 s)}{\left( \tan^2 \gamma + k_1 k_2^2 s + 1 \right)^2} \right] \quad (7)$$

where

$$s \equiv \sin(k_2\theta + \phi) \quad (8)$$

Last, the thrust angle is given by

$$\alpha = \gamma + n\pi \quad (9)$$

where  $n$  is an integer chosen so that the right-hand side of Eq. (7) is positive. When  $n = 0$ , we have thrust along the velocity vector; when  $n = 1$ , we have thrust against the velocity vector.

Equations (6) and (5), or equivalently Eq. (1), provide the circumferential and radial speeds as functions solely of position on the exponential sinusoid. Equation (7) similarly provides the normalized thrust acceleration as a function of position. Equation (6) permits retrograde motion because one need simply take the negative square root of the right-hand side to obtain  $\dot{\theta} < 0$ . However, for purposes of convenience in discussion, we examine only prograde motion here.

Considering only positive values for  $k_1$  and  $k_2$ , without loss of generality, we see from Eqs. (6) and (7) that as  $k_1 k_2^2$  approaches unity from below,  $\dot{\theta}$  and the normalized thrust acceleration both approach

infinity at periapsis (where  $s = -1$ ). For  $k_1 k_2^2 > 1$ ,  $\dot{\theta}^2$  will be less than zero in a region centered around periapsis, meaning that, in this region, the exponential sinusoid shape cannot be followed using tangential thrust. Thus, such regions of the exponential sinusoid must necessarily be avoided. Regions of high  $a$  and  $\dot{\theta}$  can also be avoided if desired, where high is to be determined by the mission designer, who should bear in mind, of course, that this is a heuristic method and so some leeway should be given for thrust-acceleration levels to exceed the capabilities of the intended thruster. The mission designer's specification of what  $a$  and  $\dot{\theta}$  are considered high will translate into a cap on the value of  $k_1 k_2^2$ .

The effects on the exponential sinusoid of a cap on the value of  $k_1 k_2^2$  are most easily understood by looking at two extremes. First, we consider the effect on the geometry. When  $k_1$  is large, that is, apoapsis is much greater than periapsis (large dynamic range),  $k_2$  must be small, meaning that many revolutions around the central body are required between periapsis and apoapsis. Conversely, when  $k_2$  is large, meaning that few, if any, revolutions are required between periapsis and apoapsis,  $k_1$  must be small, that is, apoapsis is not much greater than periapsis (small dynamic range).

Second we look at the effect of the  $k_1 k_2^2$  cap on the velocity profile. An intuitive way to assess the effect is to compare the velocity on the exponential sinusoid with the circular orbit velocity at the local radius. In the many-revolution case (small  $k_2$ ), the velocity on the exponential sinusoid is not much different from the local circular orbit velocity, particularly so at periapsis and apoapsis of the exponential sinusoid. Launching from, or effecting rendezvous at, a body in circular orbit would, thus, be most effective at periapsis or apoapsis of the many-revolution exponential sinusoid, while a gravity assist at a body in circular orbit would be most effective somewhere between periapsis and apoapsis, where the exponential sinusoid velocity is most different from the circular velocity. In the few-, or no-, revolution case (large  $k_2$ ), the exponential sinusoid velocity is significantly noncircular, making this case attractive for gravity assists at bodies in circular orbits. For a body in an orbit of medium to high eccentricity, low  $v_\infty$  values can be achieved only in the few-, or no-, revolution case, meaning that the exponential sinusoid must have a small dynamic range; high  $v_\infty$  values are easily achievable in both the few- and the many-revolution case. Further details are described by Petropoulos.<sup>23</sup>

We turn now to the matter of incorporating the exponential sinusoid with tangential thrust into a computational program. For simplicity in discussion, we consider the sun as the central body and the planets as flyby bodies, although of course the methodology applies to other central body systems, such as Jupiter and its moons. The motion of the spacecraft between planets, that is, on each leg, is permitted either to be purely conic (coasting), or to involve some degree of thrusting. The purely conic legs are computed using the previously existing capabilities of STOUR for analytic, two-body motion. The remainder of this section describes how thrust legs are computed.

In STOUR-LTGA, legs can include thrust arcs in three ways: Either the entire leg is a thrust arc, or a thrust arc is succeeded or preceded by a coast arc. In other words, the legs may be described as thrust, thrust-coast, or coast-thrust. The motion on thrusting arcs is considered in two separate parts, the in-plane motion and the out-of-plane motion. The in-plane thrusting motion is assumed to follow an exponential sinusoid [Eq. (1)] with tangential-thrust. The gravity assist is modeled as an instantaneous change in heliocentric spacecraft velocity without change in heliocentric position.

The out-of-plane motion is based on an analysis of the orbital angular momentum vector, where the out-of-plane position angle and speed are approximated from the in-plane angular momentum and velocity components. These approximations are increasingly better, the smaller the out-of-plane angles. The in- and out-of-plane motions are described in the following two subsections.

### In-Plane Motion

#### Thrust Legs

The STOUR-LTGA program steps through discrete values of the launch dates and the launch hyperbolic excess velocity  $v_\infty$  magni-

tudes specified by the user and for each value computes trajectories that reach the next body. The launch  $v_\infty$  is assumed to lie in the body's orbit plane but may point in any direction. In the case of a flyby, a B-plane angle<sup>27</sup> of 0 or 180 deg is assumed (the fundamental plane being taken as the flyby body's orbit plane), and the  $v_\infty$  turn angle is constrained by altitude. The low-thrust reference plane, that is, where the planar motion occurs, for the next leg is taken as normal to the spacecraft's initial angular momentum vector. The program steps through the full range of in-plane orientations for the outgoing  $v_\infty$ . For each outgoing  $v_\infty$ , there corresponds a heliocentric flight-path angle and speed, which means that  $\tan \gamma$  and  $\dot{\theta}$  are known. Hence, the quantity

$$k_{12s} \equiv k_1 k_2^2 s \quad (10)$$

can be determined from Eq. (6). Then, together with the trigonometric identity  $\sin^2 \theta + \cos^2 \theta \equiv 1$  and Eq. (5), there results the constraint relationship

$$k_1^2 k_2^4 - k_2^2 \tan^2 \gamma - k_{12s}^2 = 0 \quad (11)$$

between the as yet undetermined shape parameters  $k_1$  and  $k_2$ . Thus, there remains one free-shape parameter, taken as  $k_2$ , which is used to target the next body.

The search over  $k_2$  to meet the target body is narrowed in several ways. Without loss of generality, only positive values are considered for  $k_1$  and  $k_2$ . To avoid singularities around periapsis, we require

$$1 - k_1 k_2^2 > 0 \quad (12)$$

which ensures that the denominator in Eq. (6) is always positive. (When zero or negative, the exponential sinusoid cannot be followed using tangential thrust.) For practical purposes, upper limits of one and two are imposed on  $k_2$  and  $k_1$ , respectively, because the required thrust levels become untenably high when  $(1 - k_1 k_2^2)$  approaches zero. However, in the case of  $k_1$ , the user may impose a different upper limit, typically a higher one, to allow greater excursions in radial distance on legs where this may be warranted. The lower limit on  $k_2$  is taken as 0.01, as this permits up to 50 revolutions around the sun between periapsis and apoapsis, a number not likely to be exceeded in practice. Last, a range of  $k_2$  values can be determined for which the resulting exponential sinusoid will intersect the projection onto the low-thrust reference plane of the target body's orbit. For outbound targets, that is, those whose minimum projected radius  $\rho_{\min}$  is greater than the current radius  $r_B$ , we obtain, after some algebraic manipulations based on Eqs. (1) and (11),

$$k_2^2 \leq \frac{\tan^2 \gamma - 2k_{12s} \ln(\rho_{\min}/r_B)}{[\ln(\rho_{\min}/r_B)]^2} \quad (13)$$

For inbound targets, that is, those whose maximum projected radius  $\rho_{\max}$  is less than the current radius, we similarly obtain

$$k_2^2 \leq \frac{\tan^2 \gamma + 2k_{12s} \ln(r_B/\rho_{\max})}{[\ln(r_B/\rho_{\max})]^2} \quad (14)$$

For all other targets, no additional constraints can be imposed on  $k_2$ . In all cases, the limits on  $k_2$  are adjusted, if necessary, based on the limits for  $k_1$  and the constraint relationship Eq. (11).

Thus, for each turn angle we establish a range of  $k_2$  values that yield intersections of the exponential sinusoid and the projected orbit of the target. All that remains is to solve for the specific value of  $k_2$ , if any, which yields the correct TOF to the intersection. This value is found by stepping through the range of  $k_2$  values and at each step computing the location of the intersection point. Because no analytic solution is available, the intersection point is computed using a step-size and search-direction-controlled Newton method, with a suitable initial guess, as explained in subsection "Finding Intersections with the Target Body's Orbit." The TOF to the intersection is then computed by quadrature, allowing a miss angle to be found, that is, the spacecraft-sun-target angle when the spacecraft reaches the intersection point (with the target projected onto the plane). Thus, as to be explained, we search for a zero miss angle in the turn angle vs  $k_2$  space. There is a one-dimensional continuum of such solutions, which we sample at intervals according to the turn

angle and  $k_2$  step sizes. Of course, each exponential sinusoid will usually intersect the target's orbit more than once. We only keep track of up to two outbound intersections and up to two inbound intersections. We ignore subsequent intersections because they will often require inordinate amounts of propellant, or because their geometry will be similar to that of the first intersections. Thus, there is no reason to expend computation time for these intersections.

#### Thrust-Coast and Coast-Thrust Legs

For thrust-coast or coast-thrust legs, which might be termed mixed legs, the point at which the thrust is turned off or on is called the switch point. The user specifies the heliocentric radial distance of the switch point (the switch radius) and may optionally specify whether the spacecraft is to be heliocentrically inbound or outbound at the switch point (the switch direction). The default switch direction is inbound for targets that are inbound from the switch radius and is outbound for outbound targets. If the switch radius is between the target's projected apoapsis and periapsis, then both switch directions are considered by default. Multiple coast revolutions around the sun may be optionally specified.

The search for encounters with the target body is accomplished in an analogous way to the thrust-only legs, using a turn angle vs  $k_2$  search grid. For the thrusting arcs of mixed legs, the constraint relation (11) is still valid, of course. In the case of thrust-coast legs, for each turn angle in the permitted range, the upper limit on  $k_2$  is provided by Eq. (13) or Eq. (14), where the switch radius takes the place of  $\rho_{\min}$  when the switch radius is greater than  $r_B$ , or takes the place of  $\rho_{\max}$  when the switch radius is less than  $r_B$ . Intersection points and miss angles are computed as with thrust legs, except that the exponential sinusoid is replaced by a conic in seeking the intersection with the projection of the target's orbit. In the case of coast-thrust legs, for each turn angle, the spacecraft coasts to the switch point, where its state may be easily calculated, yielding a flight-path angle and speed, which are used as in the thrust-only case for determining the upper limit on  $k_2$ . Intersection points and miss angles are then computed exactly as with the thrust-only case.

#### Finding Intersections with the Target Body's Orbit

For each turn angle, the target body's orbit, assumed conic with semilatus rectum  $p$  and eccentricity  $e$ , is projected onto the low-thrust reference plane. The projected radius  $\rho$ , after a short derivation, is found to be

$$\rho = p |\cos i| / \left\{ + \sqrt{1 - \sin^2 i \cos^2 \theta} + e [|\cos i| \cos \omega \cos \theta + \operatorname{sgn}(\cos i) \sin \omega \sin \theta] \right\} \quad (15)$$

where  $i$  is the inclination with respect to the low-thrust reference plane and  $\theta$  is the polar angle in the low-thrust reference plane. The angles  $\theta$  and  $\omega$  are measured from the positive  $x$  axis, taken as the direction of the ascending node from the sun.

To find the intersection point(s)  $(r, \theta)$  of the spacecraft trajectory with the target's projected orbit, Eq. (15) must be solved with the equation for the shape of the trajectory. The shape is either the exponential sinusoid [Eq. (1)] for thrusting arcs, or the conic for coasting arcs. In both cases, the equations are transcendental in  $\theta$ , with no analytic solution readily available. Thus, the intersection point must be found by a numerical root-finding technique. A step-size- and step-direction-controlled Newton method is used to solve for the roots of the difference  $d_i$  in the inverses of the radii:

$$d_i(\theta) = 1/\rho(\theta) - 1/r(\theta) = 0 \quad (16)$$

where  $r(\theta)$  is the shape of the trajectory arc. The inverse radius is used to simplify the expression for the derivative required by the Newton method, thus, speeding up computations, convergence rates aside.

The root-finding method is best described by means of an example. We consider the intersection of an exponential sinusoid in the ecliptic plane, having periapsis at 0.8 astronomical units (AU), apoapsis at 3.1 AU, and  $k_2 = 0.1$ , with the projected orbit of the

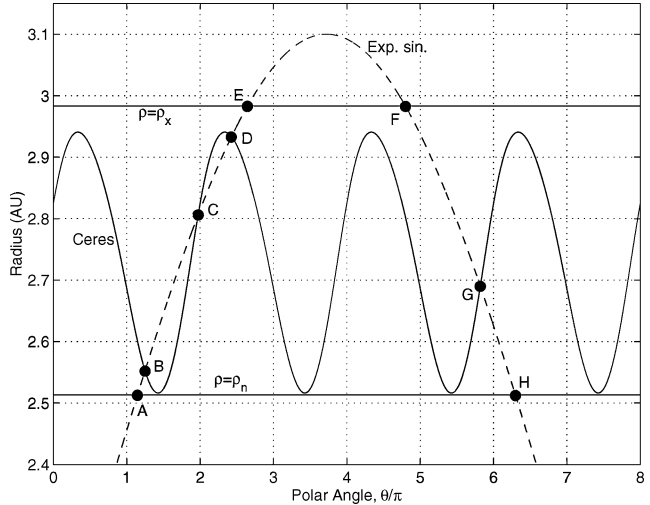


**Fig. 2** Intersections of an exponential sinusoid arc in the ecliptic with the projection of Ceres's orbit.

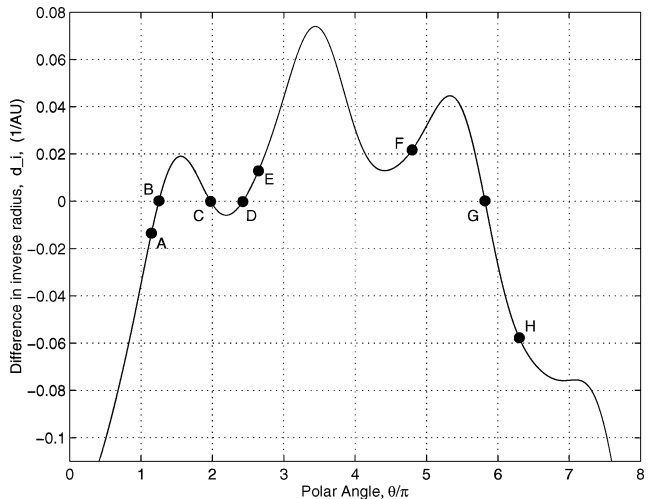


**Fig. 3** Root finding for the intersections of an exponential sinusoid with the projection of a conic section.

asteroid Ceres (semimajor axis 2.77 AU, eccentricity 0.077, and inclination 10.6 deg). For the exponential sinusoid and the projected orbit, the radius as a function of  $\theta$  is shown in Fig. 2. The difference in inverse radius  $d_i$  is shown as a function of  $\theta$  in Fig. 3. Let us assume that the spacecraft's initial position is below Ceres's orbit, that is, Ceres is outbound from the spacecraft. The sequential intersection points with Ceres's projected orbit are points B, C, D, and G in Figs. 2 and 3. The goal is to find up to two outbound and two inbound intersections, namely, points B, C, and G, respectively. (There is only one inbound intersection.)

A lower bound on the projected radius  $\rho_n$  is conservatively taken as Ceres's periapsis radius multiplied by  $|\cos i|$ . A conservative upper bound on the projected radius  $\rho_x$  is taken as Ceres's apoapsis radius itself. For the first outbound intersection (point B), the initial guess for the value of  $\theta$  solving Eq. (16) is taken as  $\theta_A$ , the easily determined value of  $\theta$  where the exponential sinusoid radius is equal to  $\rho_n$ . We note that the root is guaranteed to be beyond  $\theta_A$ . The Newton method then quickly converges to  $\theta_B$ , without any need for exercising step control. For the first inbound intersection (point G), point F, with polar angle  $\theta_F$ , is used as the initial guess. (If the exponential sinusoid's apoapsis radius is below  $\rho_x$ , then the  $\theta$  of apoapsis is used as the initial guess.) Clearly, the first step would take us away from G, and so step control is invoked, setting the next initial guess just over  $\pi/2$  beyond  $\theta_F$ . Decreases in  $\theta$  are only allowed after the first step and then only if a root of  $d_i$  is straddled. The largest permitted decrease is just under  $\pi/2$ . Thus, convergence

to the first outbound and the first inbound intersections is relatively robust.

The second outbound intersection (point C) is computed with less certainty of convergence. The initial guess is taken as the lesser of  $(\theta_B + 0.1 \text{ rad})$  and  $(4\theta_B + \theta_G)/5$ . Except in rare circumstances, the former value will normally be the lesser of the two. The same step controls as for the first intersections are still imposed. With these step controls and initial guess, if point C is too close to point B, it is skipped, with the algorithm converging to the next intersection (point D) if any. In a sense, this skipping weeds out intersections that have similar characteristics due to proximity. The second inbound intersection, which in the depicted case does not exist, is found by using  $(\theta_G + 0.1 \text{ rad})$  as the initial guess. The sampling of up to a total of four intersections, with their differing characteristics, is deemed to be sufficiently representative of the available solutions.

Although the root-finding example concerns an outbound target body, the root finding for inbound targets is entirely analogous. Also, the case where the spacecraft is on a conic arc, rather than an exponential sinusoid arc, is treated similarly, although the problem is somewhat simpler because the angular period of the spacecraft is equal to the angular period of the target body ( $2\pi$ ), whereas on an exponential sinusoid, the spacecraft's angular period can be significantly greater than the target's.

#### Grid Search for Encounters with the Target Body

Once the intersection points between the trajectory and the target's orbit have been computed for a given turn angle (TA) and  $k_2$ , the TOF to these intersections is computed by quadrature. Thus, when the spacecraft arrives at an intersection, the projected position of the target body is known, making it possible to compute the angle subtended at the sun by the spacecraft and the projected position. This miss angle is taken as positive when the target leads the spacecraft, negative when it lags. An encounter occurs when the miss angle is zero.

The process by which encounters are found may be depicted graphically, by plotting the miss angle vs  $k_2$ , with contours for different turn angles. Of course, the miss angles on any one plot should come from the same type of intersection, for example, the first outbound intersection, or the first inbound intersection. Figure 4 shows such a plot for the first outbound intersection of a Mars–Ceres leg of an Earth–Mars–Ceres trajectory with thrust-only legs. Only a representative sample of TA contours is shown.

The miss angles are computed for points on each TA contour in turn, starting at the lower end of the available  $k_2$  range for the contour. Extrapolation for zero miss angle is done both across TA contours and along TA contours. If two points on a contour straddle a zero miss angle (such as points D and E in Fig. 4), then a

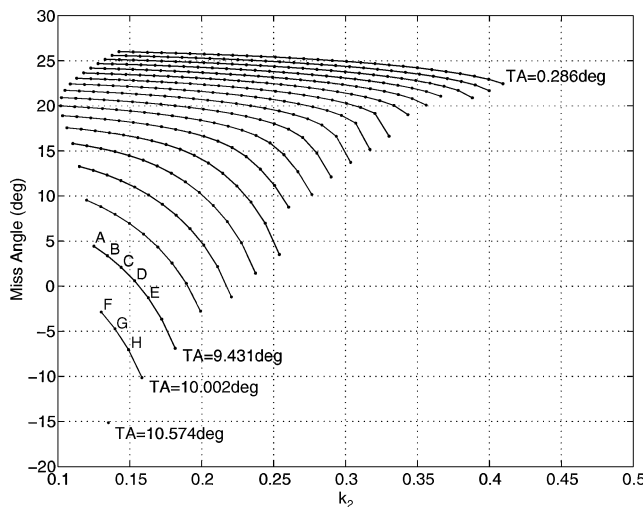


Fig. 4 Miss angle as a function of  $k_2$  with TA contours at 0.572-deg increments for exponential sinusoid arcs originating at Mars and intersecting Ceres's projected orbit.

linear extrapolation is made over  $k_2$ . The miss angle for the extrapolated value is then computed; it is retained if it falls within a certain tolerance of zero. When the next TA contour is computed, extrapolations are made between it and the previous contour, if warranted. For example, point F is closest in  $k_2$  value to point B on the previous TA contour, and the two points straddle a zero miss angle, warranting extrapolation. First a linearly extrapolated value is obtained for the turn angle, ignoring differences in  $k_2$ . The second linear extrapolation is between the  $k_2$  values of points B and F, but for the extrapolated TA value. The actual miss angle for the extrapolated TA and  $k_2$  is again checked against the tolerance. The remaining points on the contours are similarly evaluated for root straddling.

To reduce the computational memory requirements, at any one time, information is only stored for up to two TA contours. For example, the third TA contour will overwrite the first because the first is no longer needed. We note that separate miss-angle calculations must be made for the separate cases of different intersections, different switch directions, and different full coast revolutions.

#### Out-of-Plane Motion

Two cases must be distinguished. The spacecraft may encounter the target body while either on a thrust arc or on a coast arc. In both cases, the target's out-of-plane position at the time of the in-plane encounter is matched by using an additional thrust acceleration  $f_h$  acting along or against the spacecraft's angular momentum vector for some final portion of the leg's thrust arc. This out-of-plane thrust is assumed to have the form

$$f_h = [a_{0P} + b_0(r_{\min}/r)](\mu/r^2) \quad (17)$$

where  $a_{0P}$  and  $b_0$  are constants and  $r_{\min}$  is the periapsis radius of the exponential sinusoid being followed. The positive  $f_h$  direction is taken to be along the angular momentum vector. The functional form of Eq. (17) is chosen so that  $f_h$  drops off at least as fast as  $1/r^2$ , conforming to the rate at which solar power drops off.

Because both the in- and out-of-plane thrust will be much smaller than the gravitational attraction of the central body, the in-plane components of the specific angular momentum,  $h_x$  and  $h_y$ , behave according to

$$\frac{dh_x}{d\theta} \approx \frac{rf_h \sin \theta}{\dot{\theta}} \quad (18)$$

$$\frac{dh_y}{d\theta} \approx -\frac{rf_h \cos \theta}{\dot{\theta}} \quad (19)$$

where the  $x$  direction is taken as lying along  $\theta = 0$ . We note that to first order, the in-plane thrust does not affect the in-plane angular momentum components. Now,  $h_x$  and  $h_y$  remain small, so that the total angular momentum is approximately equal to just the out-of-plane component,  $r^2\dot{\theta}$ , computed as if  $f_h$  were zero. Thus, at any point on an out-of-plane thrust arc, the out-of-plane angle  $\phi$  and the speed normal to the plane,  $v_z$ , can be approximated as

$$\tan \phi \approx -(h_x \cos \theta + h_y \sin \theta)/r^2\dot{\theta} \quad (20)$$

$$v_z \approx [h_x(\sin \theta - \tan \gamma \cos \theta) - h_y(\cos \theta + \tan \gamma \sin \theta)]/r \quad (21)$$

For the thrust-to-encounter case, only the target's out-of-plane position is matched, which means that only Eq. (20) need be satisfied and not Eq. (21). Setting  $b_0 = 0$  and keeping only the unknown constant  $a_{0P}$  in the expression for  $f_h$  is sufficient to do so uniquely. For the coast-to-encounter case, both an out-of-plane speed and position must be matched at the end of the preceding thrust arc, if the spacecraft is to match the target's out-of-plane position at the end of its coast arc. Thus, in this case, both  $a_{0P}$  and  $b_0$  are needed in the expression for  $f_h$  because two equations, Eqs. (20) and (21), must be satisfied.

Because the integrals  $h_x$  and  $h_y$  in Eqs. (20) and (21) must be computed numerically, they are evaluated backward from the in-plane intersection with the target, to permit, at each integration step, the evaluation of the required  $f_h$ . The best  $f_h$  is the one used. In the

case of thrust-to-encounter best means the  $f_h$  with the lowest  $a_{0P}$ . For the coast-to-encounter case, best means the  $f_h$  with the lowest average value of  $|f_h r^2 / \mu|$ , with the average computed over  $\theta$ .

The effect of the out-of-plane motion on the TOF is ignored. This approximate method permits rapid computations and is increasingly accurate for smaller out-of-plane excursions. Although this method is incorporated into STOUR-LTGA, we generally give little consideration to the out-of-plane thrust and associated propellant because, other than a simple selection process for the out-of-plane thrust, this method is developed with regard neither for attaining the most satisfactory thrust profile nor for the benefits to be had by using different B-plane angles, that is, values other than 0 or 180 deg.

### Propellant Consumption

An estimate of the propellant consumption is made by assuming a constant specific impulse  $I_{sp}$  for the low-thrust engines. This simplification permits the required propellant mass to be expressed as a fraction of the initial spacecraft mass, based on the time integral (computed by quadrature) of the thrust acceleration and the rocket equation. In addition, we compute separately the propellant fractions required for the in-plane and out-of-plane thrust; from these we then compute a single, overall fraction. Because our approach directly determines only the shape of the trajectory, the required thrust may fall outside the range of more accurate thruster models, such as those used by Sauer.<sup>13</sup> This fact, together with the additional computational burden required by more accurate thruster models, prompt the constant  $I_{sp}$  assumption. More sophisticated models can be employed in the optimization of specific trajectories selected from the broad searches permitted by our method.

### Automated Leg Selection and Recording of Results

At any body, with a given incoming trajectory, there exists for the next leg a whole continuum of trajectory solutions in the TA vs  $k_2$  space. STOUR-LTGA samples this continuum at intervals. From each of these sampled solutions, there again arises a continuum of solutions to the next body. Thus, STOUR-LTGA limits the selection of solutions based on various criteria, to avoid a geometric increase in the number of trajectories that reach the final body. Solutions for a given leg are stored and propagated if, for example, they have the lowest TOF, the lowest propellant mass fraction, the lowest thrust levels, the lowest arrival  $v_\infty$ , the highest arrival  $v_\infty$ , and so on. Currently, the program uses 18 criteria, which can be activated or deactivated individually for each leg. Once all solution branches are propagated for one launch date and launch  $v_\infty$  pair, STOUR-LTGA begins searching for trajectories for the next pair according to the ranges and step sizes specified in the input file.

Any trajectories found by STOUR-LTGA are printed chronologically by launch date to a computer file with a one- or two-line listing for each leg of the trajectory. The listing includes, amongst other things, the shape parameters for the leg, the flyby altitude and  $v_\infty$ , the propellant mass fraction consumed, information on the thrust-acceleration levels, and flight times. The user may request that partial trajectories be printed also. In this case, for launch date and launch  $v_\infty$  values where the final body in the path could not be reached, leg data are printed up to the last body reached. The output file for a broad search often contains thousands of trajectories.

At the request of the user, for every trajectory found, STOUR-LTGA can divide the legs into segments of equal duration (where the user can select how many for each leg) and list the  $\Delta V$  accumulated on each segment due to the thrust, if any. Such output is useful as input for trajectory optimization software that uses direct methods.

## Results

The new STOUR-LTGA program can be applied<sup>23</sup> to a variety of mission design problems. As representative missions, we present here a rendezvous mission from Earth (E) via Mars (M) to the asteroid Ceres (C), and a flyby mission from E to Jupiter (J) after flybys of Venus (V), E, and M. For ease of reference, Table 1 lists the semimajor axis, eccentricity, and inclination for the heliocentric orbit of each body.

**Table 1 Orbital elements for selected bodies**

Body	Semimajor axis, AU	Eccentricity	Inclination, deg
Venus	0.72	0.007	3.4
Earth	1.00	0.017	0.0
Mars	1.52	0.093	1.8
Jupiter	5.20	0.049	1.3
Ceres	2.77	0.077	10.6

A propellant-optimal instance of the EMC mission type is presented by Sauer.<sup>13</sup> However, our EVEMJ mission type appears to be new as a low-thrust trajectory utilizing gravity assist at three distinct bodies. Selected EMC and EVEMJ trajectories from the broad searches conducted with STOUR-LTGA are used as initial estimates in optimization of the propellant consumption. We use an optimization program that is based on the direct method described by Sims and Flanagan of the Jet Propulsion Laboratory,<sup>14</sup> who made their prototype program available to Purdue. The program was rewritten at Purdue and is called the Gravity-Assist, Low-Thrust, Local Optimization Program (GALLOP).<sup>28</sup>

### Optimization Procedure in GALLOP

In the Sims–Flanagan method<sup>14</sup> used by GALLOP, the low-thrust arc is modeled as a series of segments, each one having a  $\Delta V$  impulse at its midpoint, with conic motion assumed between the impulses. Each impulse is constrained in magnitude by the flight time spent on the segment, the spacecraft mass, the thruster characteristics, and the power available to the thruster. For the GALLOP runs presented here, we assume that the thrust  $T$  and propellant mass flow rate  $\dot{m}$  are functions of power  $P$ ,

$$T = -1.9137 + 36.242P \quad (22)$$

$$\dot{m} = 0.47556 + 0.90209P \quad (23)$$

The power, assumed to come from solar panels, is in turn given as a function of distance from the sun  $r$  (measured here in astronomical units),

$$P = \frac{P_0}{r^2} \left( \frac{1.1063 + 0.1495/r - 0.299/r^2}{1 - 0.0432r} \right) \quad (24)$$

where  $P_0$  is the reference power for the solar array, roughly equal to the power produced at 1 AU. The thruster is assumed to need at least 0.649 kW of power to operate, while not being able to use power in excess of 2.6 kW. The thruster and array parameters of Eqs. (22–24) are the same as those used by Williams and Coverstone-Carroll<sup>29</sup> in modeling the engine used on Deep Space 1 and a conventional solar array. Sauer<sup>13</sup> uses similar values for the parameters.

To commence optimization on a given trajectory, GALLOP clearly requires an initial guess for the magnitude and direction of each  $\Delta V$  impulse, for the launch, flyby, and arrival dates and for the spacecraft mass and velocity at each body. All of these are available from STOUR-LTGA. Normally, STOUR-LTGA is first run in “terse” mode, where only a few details are listed for each trajectory that is found. The trajectories of the broad search are screened, and the most promising ones are rerun in STOUR-LTGA’s “verbose” mode, to produce all of the quantities needed as input to GALLOP. We emphasize that STOUR-LTGA pays no heed to actual thruster and array characteristics in computing trajectories because the thrust acceleration level is fully determined by the shape parameters and the out-of-plane approximations. It is the selection of a suitable shape and the selection of suitable parameters for that shape that permit the shape-based approach to provide approximations to low-thrust trajectories employing real electric thrusters or other low-thrust devices. Recall also, that to quantify easily the propellant expended, STOUR-LTGA assumes a constant  $I_{sp}$ , allowing the propellant mass to be expressed as a fraction of the initial spacecraft mass. In other words, apart from optimization, it is also GALLOP’s role to eliminate any violations by the initial guess of the constraints imposed by the thruster and solar array models of Eqs. (22–24).

**Table 2** STOUR-LTGA and optimal EMC trajectories

Parameter	STOUR-LTGA	GALLOP	SEPTOP	Sauer <sup>13</sup>
Launch date	6 May 2003	6 May 2003	6 May 2003	8 June 2003
Launch $v_\infty$ , km/s	1.60	1.60	1.60	1.37
M flyby $v_\infty$ , km/s	1.435	1.919	1.920	N/A
M flyby altitude, km	5432	200	200	N/A
M flyby B-plane angle, <sup>a</sup> deg	2.3	82.3	80.9	N/A
Ecliptic arrival $v_\infty$ , km/s	0.237	0.000	0.000	0.000
Propellant mass fraction	0.256	0.2335	0.2336	0.275
TOF EM, days	271	271	271	250
TOF MC, days	862	862 <sup>b</sup>	862 <sup>c</sup>	845
TOF total, days	1133	1133 <sup>b</sup>	1133 <sup>c</sup>	1095

<sup>a</sup>Fundamental plane taken as the ecliptic.

<sup>b</sup>Arrival at C actually occurs 1010 days after launch.

<sup>c</sup>Arrival at C actually occurs 970 days after launch.

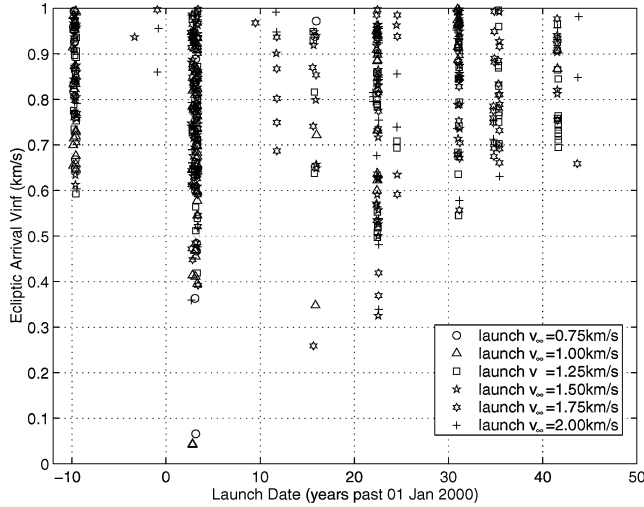


**Fig. 5** Ecliptic arrival  $v_\infty$  below 1 km/s for EMC trajectories launching between 1990 and 2049.

#### Earth–Mars–Ceres (EMC) Test Case

A broad, STOUR-LTGA search over the launch years 1990–2049, with launch  $v_\infty$  between 0.75 and 2.00 km/s, reveals that the year 2003, the month of April in particular, has one of the higher concentrations of low ecliptic arrival  $v_\infty$  trajectories. Both legs are assumed to be thrust-only legs. About 2500 trajectories are found in the broad search. Roughly 300 of these have ecliptic arrival  $v_\infty$  below 1 km/s and are shown in Fig. 5 as a scatter plot of the ecliptic arrival  $v_\infty$  against the launch date. (The ecliptic arrival  $v_\infty$  is the magnitude of the projection of the  $v_\infty$  onto the ecliptic.) The April launch date is close to that of an EMC rendezvous trajectory optimized by Sauer.<sup>13</sup> Thus, a more focused search is performed over the months of April and May 2003, with launch  $v_\infty$  between 1.0 and 1.7 km/s. From the more than 1000 trajectories found in the refined search, we select the trajectory with the lowest ecliptic arrival  $v_\infty$ , but with flight time not exceeding about 3 years. In particular, whereas the broad search produced trajectories with ecliptic arrival  $v_\infty$  values below 0.1 km/s (Fig. 5), these and similar trajectories in the refined search had flight times considerably longer than 3 years. Pertinent data are shown in Table 2 for the selected STOUR-LTGA trajectory; a trajectory plot is shown in Fig. 6. An  $I_{sp}$  of 3000 s is assumed for the propellant mass fraction.

The selected trajectory from STOUR-LTGA is used as an initial estimate in optimization using GALLOP. The optimization seeks to maximize final spacecraft mass at the rendezvous with Ceres, while keeping launch  $v_\infty$ , and launch, arrival, and flyby dates fixed at the STOUR-LTGA values. The solar array reference power  $P_0$  is taken as 10 kW, and the spacecraft initial mass as 568 kg. GALLOP converged easily to the solution summarized in Table 2. As independent verification of the optimality of the GALLOP solution, the same op-

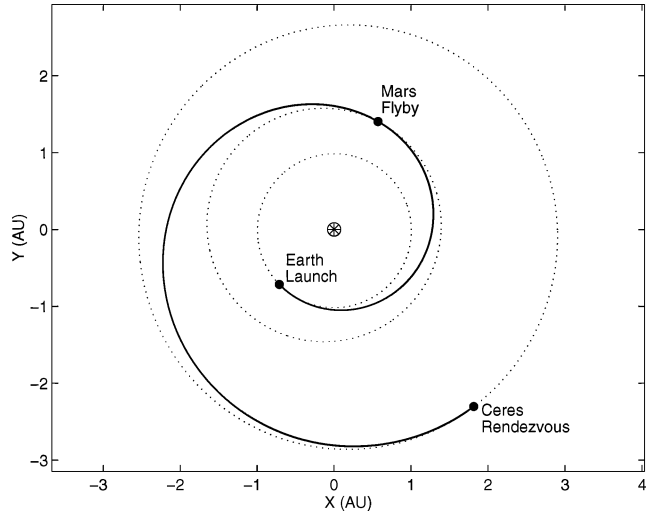


**Fig. 6** Ecliptic projection of an STOUR-LTGA EMC trajectory.

timization problem was solved using the Solar Electric Propulsion Trajectory Optimization Program (SEPTOP) developed by Sauer<sup>13</sup> and based on the calculus of variations. The initial guesses for the costate values in SEPTOP were made by trial and error because neither STOUR-LTGA nor GALLOP are able to provide the costate values. The SEPTOP solution, summarized in Table 2, is seen to be very close to the GALLOP solution. Of note is that both the GALLOP solution and the SEPTOP solution rendezvous with Ceres earlier than the requested, STOUR-LTGA time of 1133 days, as indicated in Table 2. Because the gravity of Ceres is ignored, the spacecraft remains at Ceres as they move around the sun, which means that, at the requested flight time of 1133 days, the spacecraft's position and velocity continue to match those of Ceres.

For the STOUR-LTGA trajectory and for the SEPTOP trajectory, the thrust acceleration is shown in Fig. 7 as a function of time. The out-of-ecliptic angle of the thrust direction is shown in Fig. 8. (No angle is shown where there is no thrust.) The first obvious difference in thrust profile is that the STOUR-LTGA solution has continuous thrust, whereas the SEPTOP solution has periods of coasting. The SEPTOP thrust acceleration is either at the maximum attainable by the thruster or at zero. The second main difference is that the thrust acceleration required by the STOUR-LTGA trajectory is mostly below the maximum level attainable by the thruster used in SEPTOP, but briefly above this level after the 100-day mark. The third main difference is in the profile for the out-of-plane angle.

In addition to the differences in thrust profile between the STOUR-LTGA and SEPTOP trajectories, there are somewhat prominent differences in the Mars flyby  $v_\infty$ , altitude, and B-plane angle (Table 2). In spite of the thrust and flyby differences, the propellant mass fraction for the STOUR-LTGA trajectory is only about 10% different from the optimal value found by GALLOP.

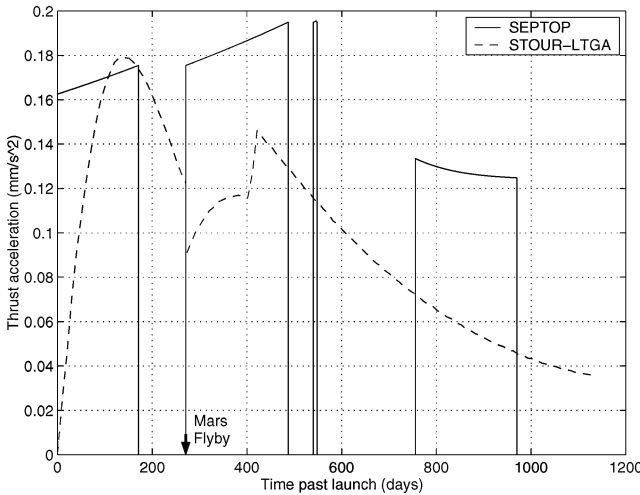


Fig. 7 Thrust acceleration for STOUR-LTGA and SEPTOP EMC trajectories.

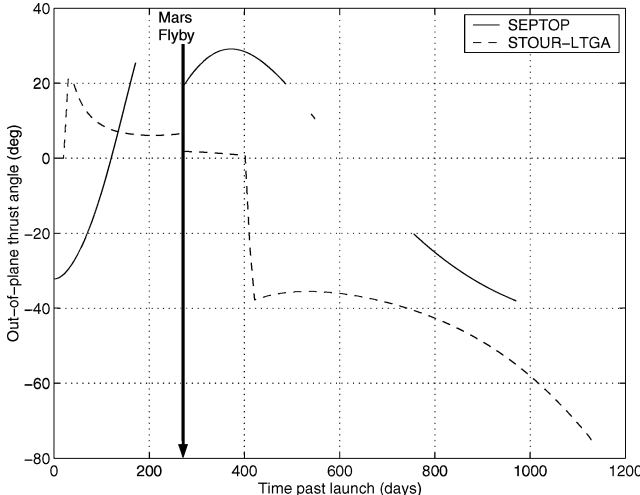


Fig. 8 Out-of-ecliptic thrust angle for STOUR-LTGA and SEPTOP EMC trajectories.

and SEPTOP (Table 2). Given the heuristic assumptions made in STOUR-LTGA for the trajectory dynamics, one might have expected the difference to be larger.

Sauer<sup>13</sup> presents a propellant-optimal EMC rendezvous trajectory, also computed using SEPTOP, in which two thrusters are used, the reference power is 10 kW, the initial mass is 1123 kg, and the spacecraft consumes 250 W for housekeeping. Available data for this trajectory are shown in Table 2. The launch, flyby, and arrival dates are free in the optimization. The launch  $v_\infty$  is also free, but dictates the initial spacecraft mass according to the performance of the launch vehicle used. We see that, although the optimization problem solved by Sauer is somewhat different from the one solved with GALLOP and SEPTOP based on the STOUR-LTGA solution, there is a general correspondence in the solutions.

#### Earth–Venus–Earth–Mars–Jupiter (EVEMJ) Test Case

In the literature, the optimal trajectories we have found have, at most, two flybys on thrusting legs between departure and destination planets. STOUR-LTGA, in addition to the strength of broad searching over launch date and  $v_\infty$ , offers the significant ability of searching over different, long sequences of flyby bodies. One such path is EVEMJ (including launch and destination bodies). Currently, paths of up to 20 bodies are permitted, although this limit can be easily increased. Of course, the longer the paths, the longer the computation times, and the longer the flight times, making the longer paths better suited for short-period bodies.

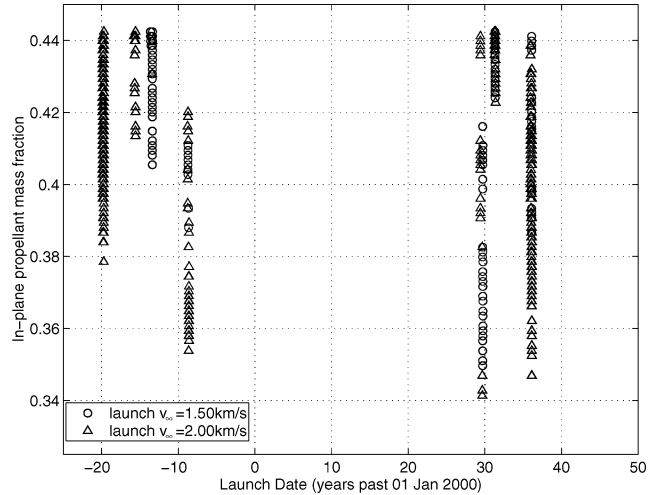


Fig. 9 In-plane propellant consumption for EVEMJ trajectories.

For the EVEMJ path, where a flyby of Jupiter is desired, the launch years 1975–2049 are searched, for launch  $v_\infty$  of 0.5–2 km/s at 0.5 km/s increments. These launch  $v_\infty$  values are well below the Hohmann launch  $v_\infty$  to Venus (2.5 km/s). The MJ leg is assumed to be a thrust–coast leg, with a switch radius of 3 AU, a distance where large solar panels would be needed to power a thruster. The other three legs are assumed to be thrust-only legs. To keep the search times short, a launch-date step of 10 days is used. Because the last leg, the MJ leg, will be somewhat energetic, the upper limit on  $k_1$  is set to 3. A maximum total time of flight of 2500 days is allowed, with the maximum leg flight times set at 500 days for each leg except the MJ leg, which is allowed up to 2000 days. The minimum flyby altitudes at the gravity-assist bodies are all 200 km. Finally, with an  $I_{sp}$  of 3000 s assumed, conservative caps of 0.385 and 0.25 mm/s<sup>2</sup> and 0.35 mm/s<sup>2</sup> are set on the in-plane propellant mass fraction and the average and maximum thrust accelerations, respectively. These caps are set somewhat higher than the values that might be desired or available on a real mission to account for possible excesses required by the tangential-thrust exponential sinusoid.

The broad search yields two main groupings of trajectories, spaced about 49 years apart, as seen in Fig. 9, where the in-plane propellant mass fraction is plotted against launch date. The 49-year spacing corresponds roughly with the 45-year repeat cycle noted in previous work<sup>30</sup> for the ballistic EVMVEJ path with the same flyby bodies. Trajectories are found only for launch  $v_\infty$  of 1.5 and 2 km/s, where there are about four times as many 2-km/s trajectories as 1.5-km/s trajectories. Higher launch  $v_\infty$  and less restrictive constraints on the thrust levels would fill out the trajectory families and produce new ones.

We select, from the broad search, the trajectory with the lowest in-plane propellant mass fraction, which launches in 2029, because it also has attractive thrust and flight time characteristics when compared to the other trajectories in the 2029–2036 trajectory grouping. The trajectory geometry is shown in Fig. 10, and pertinent data are listed in Table 3. The trajectory also serves as an initial estimate in optimization using GALLOP, where the maximum final mass is sought for a fixed launch mass of 300 kg and where a reference array power of 10 kW is used. The launch  $v_\infty$ , launch, flyby, and arrival dates are all held fixed at the STOUR-LTGA values, except for the E flyby date, which is moved 16 days earlier, as to be explained. The propellant optimal trajectory found by GALLOP is also reported in Table 3.

When the unoptimized and optimized trajectories in Table 3 are compared, three main differences are seen. First, the B-plane angles are different, significantly so in the case of Venus, which means that the optimizer was able to alter these to effect the out-of-plane targeting more efficiently than using thrust alone. The more efficient out-of-plane motion in the optimized trajectory is also evident in that the STOUR-LTGA propellant mass fraction for the in-plane

**Table 3** STOUR-LTGA EVEMJ trajectory and its GALLOP-optimized version

Parameter	STOUR-LTGA	GALLOP
Launch date	3 Sept. 2029	3 Sept. 2029
Launch $v_\infty$ , km/s	2.00	2.00
V flyby $v_\infty$ , km/s	3.64	3.77
V flyby altitude, km	6,533	30,000
V flyby B-plane angle, <sup>a</sup> deg	178.3	60.7
E flyby $v_\infty$ , km	6.50	5.18
E flyby altitude, km	655	1,035
E flyby B-plane angle, <sup>a</sup> deg	-180.0	-176.5
M flyby $v_\infty$ , km/s	13.70	11.26
M flyby altitude, km	200	200
M flyby B-plane angle, <sup>a</sup> deg	-1.8	-5.5
J flyby $v_\infty$ , km/s	5.85	6.25
Average thrust acceleration, EV, mm/s <sup>2</sup>	0.12	N/A
Average thrust acceleration, VE, mm/s <sup>2</sup>	0.16	N/A
Average thrust acceleration, EM, mm/s <sup>2</sup>	0.10	N/A
Average thrust acceleration, MJ, mm/s <sup>2</sup>	0.14	N/A
Switch radius, AU	3.0	N/A
Propellant mass fraction	0.408	0.256
Propellant mass fraction, in-plane only	0.294	N/A
TOF EV, days	165	165
TOF VE, days	334	318
TOF EM, days	131	147
TOF MJ, days	1,335	1,335
TOF Total, days	1,965	1,965

<sup>a</sup>Fundamental plane taken as the ecliptic.

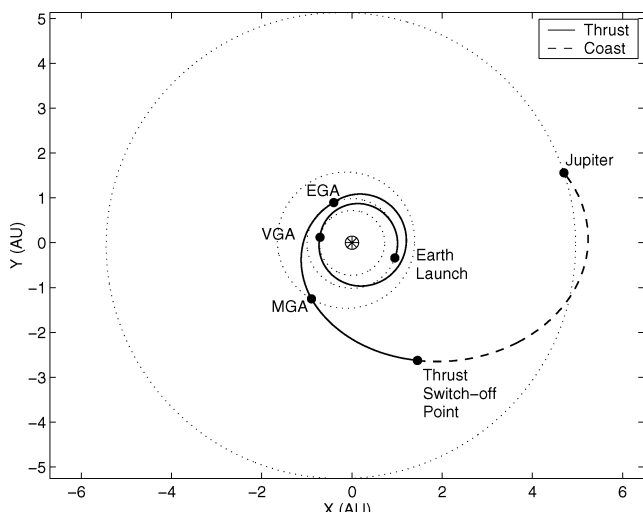


**Fig. 10** Ecliptic projection of an STOUR-LTGA EVEMJ trajectory; E, V, and M gravity assists are labeled EGA, VGA, and MGA, respectively.

thrusting is only 15% greater than the optimized overall propellant mass fraction, compared to 60% greater for the STOUR-LTGA in- and out-of-plane propellant mass fraction. Second, the flyby altitude at Venus is almost five times larger in the optimized case. Third, the flyby date of Earth in the optimized case is 16 days before that in the unoptimized case. The last two differences are present largely as a way of reducing the lengthy (and wasteful) thrusting excursion beyond 1 AU, exhibited by the unoptimized trajectory prior to the Earth flyby (Fig. 10). One potential method of diminishing this excursion in STOUR-LTGA would be to use a thrust-coast leg for the VE transfer. As for the considerably higher, optimized Venus flyby altitude, it still causes the incoming  $v_\infty$  to be turned by 46 deg, corresponding to a heliocentric  $\Delta V$  of 2.93 km/s. We note that GALLOP did not converge as easily on this EVEMJ trajectory as it did on the EMC trajectory (Table 2). Perhaps the added difficulty is due to the added complexity of not only imposing two more flyby constraints, but also of determining how to use the flybys most effectively. Last, both the optimized and unoptimized ver-

sions of this EVEMJ trajectory are seen to be comparable to, if not superior to, ballistic, gravity-assist EJ trajectories previously reported.<sup>30</sup>

### Other Paths

When using STOUR-LTGA, the LTGA mission designer is faced with yet another choice: which trajectory path to use. In this paper, we have discussed a simple path and a more complex path. Other complex paths of similar character, such as EVMVEJ, can be easily identified. One class of transfers deserving special mention is that of consecutive flybys of the same body for  $v_\infty$ -leveraging purposes.<sup>31</sup> (With interior leveraging, after a flyby or launch, a small  $\Delta V$  is applied near periaxis to increase the  $v_\infty$  of the next flyby. With exterior leveraging, a similar effect is achieved by applying the  $\Delta V$  near apoapsis.) Whether interior or exterior leveraging is sought, the transfers should be set as coast-thrust in STOUR-LTGA, as can be explained by considering a tangential launch from Earth. In both the interior and exterior cases, a thrust-coast leg will not permit a reencounter of the Earth, for typical values of the  $k_1$  and  $k_2$  parameters. In the interior case, the apoapsis of the trajectory's osculating ellipse is reduced below 1 AU, whereas in the exterior case, the periaxis is raised above 1 AU, making it impossible to return to Earth on a coast arc. Using a thrust-only leg to return to Earth would be possible, but wasteful, because the arrival  $v_\infty$  at Earth encounter would be the same as the launch  $v_\infty$  (assuming a circular Earth orbit), due to the symmetry of the exponential sinusoid. The coast-thrust leg does not have these difficulties. By extension, any transfer back to the same body, whether at launch or later in a path, should be set as a coast-thrust transfer.

### Conclusions

We present a planar shape-based method for finding LTGA trajectories from the infinity of solutions made possible by the availability of continuous thrust. Whereas the primary drawback of the shape-based method is that the thrust levels are determined a posteriori, that is, they cannot be explicitly prescribed by the mission designer, we show that there exists at least one shape, the exponential sinusoid, that not only exhibits required thrust levels that are reasonably close to those attainable in engineering practice, but also that has a velocity profile that makes it practically applicable to LTGA missions.

In particular, we use the exponential sinusoid with the assumption of tangentially directed thrust, to compute rendezvous trajectories to the asteroid Ceres via a Mars gravity assist and Jupiter flyby trajectories, using gravity assists at Venus, Earth, and Mars. Trajectories are computed in an automated way by a software program according to broad search criteria set by the mission designer. In addition to the exponential-sinusoid, low-thrust arcs, the program includes out-of-plane approximations, as well as exact, two-body, conic solutions for periods of coasting. Attractive trajectories from the broad search are passed on as initial estimates to an optimization program, which relies on direct methods. We show that even though the thrust profile of the initial estimate might differ significantly from the propellant-optimal solution, the optimizer is able to optimize the thrust profile without violating the thrust constraints, yielding a propellant mass fraction that is correlated to the initial estimate. We find that the shape-based method not only provides broad overviews of the trajectory design space, but also provides good starting points for trajectory optimization.

### Acknowledgments

This research has been supported in part by the Jet Propulsion Laboratory, California Institute of Technology under Contracts 961211 and 1211514. We are grateful to Dennis V. Byrnes (Technical Manager) and Jon A. Sims for providing useful information, guidance, and helpful suggestions. We also thank Jon Sims and Steve N. Flanagan for providing their direct-optimization computer code and T. Troy McConaghay for rewriting it and assisting us in its use. In addition, we appreciate the guidance offered to us by Carl Sauer in using SEPTOP and assistance from Theresa Debban with the optimization of the Earth-Mars-Ceres trajectory.

## References

- <sup>1</sup>Rayman, M. D., Varghese, P., Lehman, D. H., and Livesay, L. L., "Results from the Deep Space 1 Technology Validation Mission," *Acta Astronautica*, Vol. 47, Nos. 2–9, 2000, pp. 475–487.
- <sup>2</sup>Rayman, M. D., and Williams, S. N., "Design of the First Interplanetary Solar Electric Propulsion Mission," *Journal of Spacecraft and Rockets*, Vol. 39, No. 4, 2002, pp. 589–595.
- <sup>3</sup>Murrill, M. B., "The Grandest Tour: VOYAGER," *Mercury*, Vol. 22, No. 3, 1993, pp. 66–77.
- <sup>4</sup>Kawaguchi, J., Takiura, K., and Matsuo, H., "On the Optimization and Application of Electric Propulsion to Mars and Sample and Return Mission," *Advances in the Astronautical Sciences*, Vol. 87, No. 1, 1994, pp. 539–556.
- <sup>5</sup>Thorne, J. D., and Hall, C. D., "Minimum-Time Continuous-Thrust Orbit Transfers," *Journal of the Astronautical Sciences*, Vol. 45, No. 4, 1997, pp. 411–432.
- <sup>6</sup>Kluever, C. A., "Optimal Low-Thrust Interplanetary Trajectories by Direct Method Techniques," *Journal of the Astronautical Sciences*, Vol. 45, No. 3, 1997, pp. 247–262.
- <sup>7</sup>Kechichian, J. A., "Low-Thrust Trajectory Optimization Based on Epoch Eccentric Longitude Formulation," *Advances in the Astronautical Sciences*, Vol. 87, No. 2, 1994, pp. 863–884.
- <sup>8</sup>Coverstone-Carroll, V., and Williams, S. N., "Optimal Low Thrust Trajectories Using Differential Inclusion Concepts," *Journal of the Astronautical Sciences*, Vol. 42, No. 4, 1994, pp. 379–393.
- <sup>9</sup>Betts, J. T., "Optimal Interplanetary Orbit Transfers by Direct Transcription," *Journal of the Astronautical Sciences*, Vol. 42, No. 3, 1994, pp. 247–268.
- <sup>10</sup>Betts, J. T., "Survey of Numerical Methods for Trajectory Optimization," *Journal of Guidance, Control, and Dynamics*, Vol. 21, No. 2, 1998, pp. 193–207.
- <sup>11</sup>Betts, J. T., and Huffman, W. P., "Sparse Optimal Control Software SOCS," Boeing Information and Support Services, Mathematics and Engineering Analysis Technical Document MEA-LR-085, The Boeing Co., Seattle, WA, July 1997.
- <sup>12</sup>Hui, Y., and Hongxin, W., "Initial Adjoint Variable Guess Technique and Its Application in Optimal Orbital Transfer," AIAA Paper 98-4551, Aug. 1998.
- <sup>13</sup>Sauer, C. G., "Solar Electric Performance for Medlite and Delta Class Planetary Missions," American Astronautical Society, AAS Paper 97-726, Aug. 1997.
- <sup>14</sup>Sims, J. A., and Flanagan, S. N., "Preliminary Design of Low-Thrust Interplanetary Missions," American Astronautical Society, AAS Paper 99-338, Aug. 1999.
- <sup>15</sup>Petropoulos, A. E., Longuski, J. M., and Vinh, N. X., "Shape-Based Analytic Representations of Low-Thrust Trajectories for Gravity-Assist Applications," American Astronautical Society, AAS Paper 99-337, Aug. 1999.
- <sup>16</sup>Petropoulos, A. E., and Longuski, J. M., "Automated Design of Low-Thrust Gravity-Assist Trajectories," AIAA Paper 2000-4033, Aug. 2000.
- <sup>17</sup>Tsu, T. C., "Interplanetary Travel by Solar Sail," *Journal of the American Rocket Society*, Vol. 29, June 1959, pp. 422–427.
- <sup>18</sup>Lawden, D. F., *Optimal Trajectories for Space Navigation*, 1st ed., Butterworths, London, 1963, pp. 86–94.
- <sup>19</sup>Battin, R. H., *An Introduction to the Mathematics and Methods of Astrodynamics*, 1st ed. 4th printing, AIAA, New York, 1987, pp. 408–418.
- <sup>20</sup>Prussing, J. E., and Coverstone-Carroll, V., "Constant Radial Thrust Acceleration Redux," *Journal of Guidance, Control, and Dynamics*, Vol. 21, No. 3, 1998, pp. 516–518.
- <sup>21</sup>Markopoulos, N., "Non-Keplerian Manifestations of the Keplerian Trajectory Equation and a Theory of Orbital Motion Under Continuous Thrust," American Astronautical Society, AAS Paper 95-217, Feb. 1995.
- <sup>22</sup>Bishop, R. H., and Azimov, D. M., "New Analytic Solutions to the Fuel-Optimal Orbital Transfer Problem Using Low-Thrust Exhaust-Modulated Propulsion," American Astronautical Society, AAS Paper 00-131, Jan. 2000.
- <sup>23</sup>Petropoulos, A. E., "A Shape-Based Approach to Automated, Low-Thrust, Gravity-Assist Trajectory Design," Ph.D. Dissertation, School of Aeronautics and Astronautics, Purdue Univ., West Lafayette, IN, May 2001.
- <sup>24</sup>Longuski, J. M., "Galileo User's Guide (Phase 1), Mission Design System, Satellite Tour Analysis and Design Subsystem, STOUR Program Set," Jet Propulsion Lab., Document D-263, California Inst. of Technology, Pasadena, CA, Oct. 1983.
- <sup>25</sup>Williams, S. N., "Automated Design of Multiple Encounter Gravity-Assist Trajectories," M.S. Thesis, School of Aeronautics and Astronautics, Purdue Univ., West Lafayette, IN, Aug. 1990.
- <sup>26</sup>Bonfiglio, E. P., Longuski, J. M., and Vinh, N. X., "Automated Design of Aerogravity-Assist Trajectories," *Journal of Spacecraft and Rockets*, Vol. 37, No. 6, 2000, pp. 768–775.
- <sup>27</sup>Sergeyevsky, A. B., and Snyder, G. C., "Interplanetary Mission Design Handbook, Volume I, Part 3," Jet Propulsion Lab., JPL Publ. 82-43, California Inst. of Technology, Pasadena, CA, Dec. 1982, p. 20.
- <sup>28</sup>McConaghy, T. T., Debban, T. J., Petropoulos, A. E., and Longuski, J. M., "Design and Optimization of Low-Thrust Trajectories with Gravity Assists," *Journal of Spacecraft and Rockets*, Vol. 40, No. 3, 2003, pp. 380–387.
- <sup>29</sup>Williams, S. N., and Coverstone-Carroll, V., "Benefits of Solar Electric Propulsion for the Next Generation of Planetary Exploration Missions," *Journal of the Astronautical Sciences*, Vol. 45, No. 2, 1997, pp. 143–159.
- <sup>30</sup>Petropoulos, A. E., Longuski, J. M., and Bonfiglio, E. P., "Trajectories to Jupiter via Gravity Assists from Venus, Earth, and Mars," *Journal of Spacecraft and Rockets*, Vol. 37, No. 6, 2000, pp. 776–783.
- <sup>31</sup>Sims, J. A., Longuski, J. M., and Staugler, A. J., "V<sub>∞</sub> Leveraging for Interplanetary Missions: Multiple-Revolution Orbit Techniques," *Journal of Guidance, Control, and Dynamics*, Vol. 20, No. 3, 1997, pp. 409–415.

C. A. Kluever  
Associate Editor